Original Article

TIPS Trends in Pharmaceutical Sciences 2025: 11(1): 17-28.

Preparation and In-vitro Characterization of Giant Superparamagnetic Nanobeads: A Proof of Concept

Amir Reza Fatemi[1];Ph.D, Mohammad Javad Raee[2,3];Ph.D, Ali Mohammad Tamaddon[4];Ph.D, Sara Sadeghian[5];Ph.D, Salmeh Amiri[4];Ph.D, Dena Firouzabadi[6];Ph.D, Fakhrossadat Farvadi[4*];Ph.D

[1]Student Research Committee, University of Medical Sciences, Shiraz, Iran.
[2]Department of Pharmaceutical Biotechnology, School of Pharmacy, Shiraz University of Medical Sciences, Shiraz, Iran.
[3]Pharmaceutical Sciences Research Center, Shiraz University of Medical Sciences, Shiraz, Iran.
[4]Center for Nanotechnology in Drug Delivery, Shiraz University of Medical Sciences, Shiraz, Iran.
[5]Department of Medicinal Chemistry, School of Pharmacy, Shiraz University of Medical Sciences, Shiraz, Iran.
[6]Department of Clinical Pharmacy, School of Pharmacy, Shiraz University of Medical Sciences, Shiraz, Iran.

Abstract

The isolation of biomolecules from complex biological environments is a crucial step in the accurate analysis of biomarkers, which in turn is vital for enhancing the precision of medical diagnoses. Among the various techniques employed for biomarker separation, immunomagnetic separation utilizing superparamagnetic iron oxide nanoparticles (SPIONs) has emerged as a promising approach. Nonetheless, the diminutive size of SPIONs poses challenges regarding their robustness, particularly in the efficient extraction of macromolecules from diverse biological samples. This study addresses this pressing concern by investigating methods to enhance the magnetic properties of these nanoparticles. Specifically, we focus on increasing the magnetic unit size while preserving their superparamagnetic characteristics. Through a novel methodological approach, we successfully created giant superparamagnetic nanoclusters via click binding of biotinylated SPIONs with avidin macromolecules. These large nanoclusters exhibited favorable magnetic properties, indicating their potential for significant application in biomarker discovery and analysis, thus paving the way for advancements in biomedical diagnostics.

Keywords: Superparamagnetic, Nanoparticle, Nanocluster, Immunomagnetic separation

Please cite this article as: Fatemi AR, Raee MJ, Sadeghian S, Amiri S, Firouzabadi D, Farvadi F*. Preparation and In-vitro Characterization of Giant Superparamagnetic Nanobeads: A Proof of Concept. Trends in Pharmaceutical Sciences. 2025;11(1):17-28. doi: 10.30476/tips.2025.104304.1261

Copyright: ©Trends in Pharmaceutical Sciences. This is an open-access article distributed under the terms of the Creative Commons Attribution-NoDerivatives 4.0 International License. This license allows reusers to copy and distribute the material in any medium or format in unadapted form only, and only so long as attribution is given to the creator. The license allows for commercial use.

1. Introduction

Medical diagnosis (MD) serves as a crucial tool within the healthcare system to determine the most effective treatment strategies for patients. Beyond treatment, it has a significant impact on patient care, and on healthcare research and policy-making (1). Accurate and timely MD are highly influential factors in improving the quality of the "diagnosis" process in medicine (2).

The isolation and separation of different types of biomarkers from biological samples is considered a crucial step in improving the quality of MD and is used in almost all branches of biological and medical sciences such as pathology, immunology, toxicology,

Corresponding Author: Fakhrossadat Farvadi, Center for Nanotechnology in Drug Delivery, Shiraz University of Medical Sciences, Shiraz, Iran.
Email address: farvadi@gmail.com

Received: 08/04/2024; Accepted: 01/09/2024

and biotechnology (3). To date, various techniques have been developed for the isolation and separation of biomarkers from biological samples, including precipitation, chromatography, ultrafiltration and microfiltration, electrophoresis and immunofluorescence-based techniques. Despite their numerous advantages, each of these techniques has limitations and drawbacks that need to be considered. One of the most efficient techniques for separating biomarkers from biological environments is the use of ligand-modified magnetic nanoparticles, which are able to bind to the biological markers of interest and isolate them from the environment. This technique is called immunomagnetic separation (IMS) (4).

Superparamagnetic behavior is a magnetic behavior of a class of materials exhibited by magnetic nanoparticles called superparamagnetic iron oxide nanoparticles (SPIONs). When magnetic materials are synthesized at the nanometer scale, the magnetic domains are partitioned into individual nanoparticles with random magnetic orientations. Therefore, despite the strong magnetic moment and the maximum saturation magnetization of each particle, the sum of these values decreases so that the nanomaterials are unable to magnetize spontaneously (5). SPIONs have a high magnetic susceptibility. In contrast to magnetic materials, SPIONs lose their magnetism after the removal of an external magnetic field; therefore, they can act selectively and prevent aggregation (5, 6). Due to the nanometric dimensions of the particles, we have a very favorable surface-to-volume ratio for the binding of specific ligands to the surface of the nanoparticles. This potential makes SPIONs ideal for IMS (7).

The separation of biological markers by magnetic nanoparticles conjugated with specific ligands is technically simple and does not require complex equipment and extra energy. With the IMS technique, all isolation steps are carried out in a single tube. In addition, the nanoparticles can be recycled and reused (8, 9). The main advantage of IMS is its high sensitivity, specificity, and high throughput, which enables the specific separation of target biomarkers with high efficiency (8). Despite the significant advantages of IMS mentioned above, this method still has some limitations. One of the most serious limitations of the IMS technique is the small size of the SPIONS, which results in a lower maximum saturation magnetization than ferromagnetic magnets, requiring the application of a strong magnetic field for separation and consequently resulting in higher costs. The small size of the particles also means that they are absorbed by the cells, which can damage the contents of the sample (10).

One approach to overcome the size limitations of SPIONs is the formation of SPION clusters (11). The clustering of SPIONs leads to larger dimensions while maintaining the superparamagnetic properties of the particles, which in turn significantly increases the maximum saturation magnetization of the particles (12). Furthermore, despite the overall lower surface-to-volume ratio compared to single nanoparticles, they have a higher surface-to-volume ratio for binding to biomarkers than particles of the same size due to clustering. We can also control the size of iron oxide nanoclusters (IONC) more efficiently than single SPIONs (10, 11).

In this study, we intend to utilize a unique route to fabricate nanoclusters by establishing a robust bond between biotinylated nanoparticles and the macromolecule avidin, forming a biotin-avidin complex (BAC). The 3D structure of avidin provides specific binding sites for biotin so that each avidin macromolecule can bind four biotin molecules with very high affinity. The biotin-avidin bond is one of the strongest non-covalent bonds found in nature ($K_a=10^{15}M^{-1}$) (13). We hypothesize that the superparamagnetic iron oxide nanoclusters synthesized in this way have a higher saturation magnetization than single nanoparticles and can therefore isolate and separate various biomarkers from biological environments with higher efficiency. In addition, the presence of biotin on the formed nanoclusters provides a platform for the attachment of a variety of avidinylated targeting molecules.

2. Material and Methods

2.1. Materials

Avidin was purchased from Sig-

ma-aldrich®, D-biotin from Molekula®, $FeCl_3.6H_2O$ and $FeSO_4.7H_2O$ were produced by Merck®, L-lysine, N-hydroxysuccinimide (NHS) and N,N′-di cyclohexyl carbodiimide (DCC) were purchased from Bio basic®.

2.2. Synthesis and characterization of L-Lysine-magnetic iron oxide nanoparticles

Superparamagnetic iron oxide nanoparticles coated with L-lysine (Lys-SPIONs) were synthesized by a co-precipitation technique performed by Raee et al (14). First, 1.7 g of $FeCl_3.6H_2O$ and 0.6 g of $FeSO_4.7H_2O$ were dissolved in 50 ml of degassed distilled water. The system was placed in a two-necked flask, fixed in an oil bath under N_2 at 70 °C and stirred at 1000 rpm. After 30 minutes, 1.6 g of L-lysine dissolved in 6 ml of distilled water was quickly added to the system. 30 minutes later, 60 ml of 25% w/v NH_4OH was rapidly injected into the system to alkalinize the medium, and the pH reached 11.1. The system was left in this state for 90 minutes to allow Lys-SPIONs to gradually form. The synthesized Lys-SPIONs were separated with a magnet and then washed three times with warm distilled water. Finally, the purified Lys-SPIONs were dried in an oven (Father, B630).

Lys-SPIONs were characterized by DLS and Zeta-check (Nanoparticle size analyzer, Microtrac, Nanoflex), XRD (X-ray diffractometer, Malvern panalytical, X'pert Pro MPD), FT-IR (Fourier Transformed Infrared spectroscopy, Bruker, Vertex 70), TGA (Thermal gravimetric analyzer, Mettler Toledo, TGA/DSC 1STAR System) and VSM (Vibrating Sample Magnetometer, Meghnatis Danesh pazhooh Co., Kashan, Iran).

2.3. Biotinylation of Lysine-SPIONs

Step1: Synthesis of Biotin- N-Hydroxy succinimide (Biotin-NHS) as the intermediate product via DCC/NHS reaction

To synthesize the biotin-NHS compound, a 1:3:5 molar ratio of biotin, N-hydroxysuccinimide (NHS) and N,N′-di cyclohexyl carbodiimide (DCC) was prepared. First, 128 mg of biotin and 185 mg of NHS were added to 5 ml of dry dimethylformamide (DMF) as solvent. The mixture was stirred at 52 °C (in an oil bath) until the biotin and NHS were completely dissolved in DMF. Then 545 mg DCC was added and the system was allowed to stand in the dark for 24 hours. The formation of a white slurry resulting from the suspension of the reaction by-product, the dicyclohexylurea (DCU) molecule, is evidence of completion of the reaction.

To extract and purify the synthesized biotin-NHS compound, the DCU molecules were first separated using a Whatman® cellulose filter. Then biotin-NHS was precipitated with cold diethyl ether in tenfold amount as an antisolvent with constant stirring. The precipitated biotin-NHS was finally extracted after washing with diethyl ether. The purified biotin-NHS was dried at 55 °C and stored at -18 °C.

The formation of biotin-NHS was confirmed by the determination of the melting point (melting point apparatus, Electrothermal, IA9100) and 13C NMR & 1H NMR (nuclear magnetic resonance spectrometer, Bruker, NMR 300 MHz).

Step 2: Modification of Lys-SPIONs with biotin-NHS intermediate molecules

A solution of biotin-NHS in anhydrous DMSO was mixed with 400 µl of Lys-SPION and incubated at room temperature for 48 hours with stirring, according to the study of Chauhan et al. (15). The biotinylated SPIONs (Bio-SPIONs) were collected with a magnet and washed with DMF and deionized water respectively then stored in a refrigerator (2–8 °C).

The Bio-SPIONs were analyzed by DLS and Zeta-Check (nanoparticle size analyzer, Microtrac, Nanoflex), FT-IR (Fourier Transformed Infrared Spectroscopy, Bruker, Vertex 70), TEM (Transmission Electron Microscope, Carl Zeiss AG, EM 900) and TGA (Thermal gravimetric analyzer, Mettler Tole-

do, TGA/DSC 1STAR System).

2.4. Biotin-Avidin complexation and formation of superparamagnetic iron oxide nanoclusters (SPINCs)

Serial dilutions of avidin (250-1.3 µg/ml) were mixed with a fixed concentration of BIO-SPIONs (250 µg/ml) in 1X PBS with pH=7.4 (Table S1). The system was incubated on the revolver (Labnet, H5600-15) for 1 hour at room temperature. The final products were characterized by DLS and Zeta-Check (nanoparticle size analyzer, Microtrac, Nanoflex), FT-IR (Fourier Transformed Infrared spectroscopy, Bruker, Vertex 70), TEM (Transmission Electron Microscope, Carl Zeiss AG, EM 900) and VSM (Vibrating Sample Magnetometer, Meghnatis Danesh pazhooh Co.).

3. Results

3.1. Synthesis and characterization of Lys-SPION

Superparamagnetic iron oxide nanoparticles were synthesized with a hydrodynamic diameter of 67 nm (Figure 1.A). The X-ray diffraction pattern was in consistent with the Fe_3O_4 cubic inverse spinel crystal lattice (Figure 1.B). The crystal structure of Fe_3O_4 is an oxygen-packed arrangement with divalent iron ions and half of the trivalent iron ions in an octahedral coordination and the other half of the trivalent iron ions in a tetrahedral coordination (16).

The sharp absorption band in the FT-IR spectrum at 580 cm^{-1} is related to the characteristics of the Fe-O bond (Figure 1.C). The two absorption bands at 1460 cm-1 and 1623 cm-1 are due to the stretching vibrations of the C-O and C=O bonds of the carboxylic acid group of the L-lysine attached on the surface of the nanoparticles, respectively (14). Considering the narrowing of the broad peak of the Lys-SPION infrared spectrum in the 2800-3500 cm-1 region, compared to the infrared spectrum of L-lysine, L-lysine has formed an ester bond from its carboxylic acid end with the hydroxylated surface oxygen ions of iron oxide, and its terminal chain amine is free.

3.2. Vibrating-Sample Magnetometry analysis (VSM)

Figure 1.D shows the magnetization (M) curve of Lys-SPIONs versus the applied magnetic field (H) at room temperature. Ac-

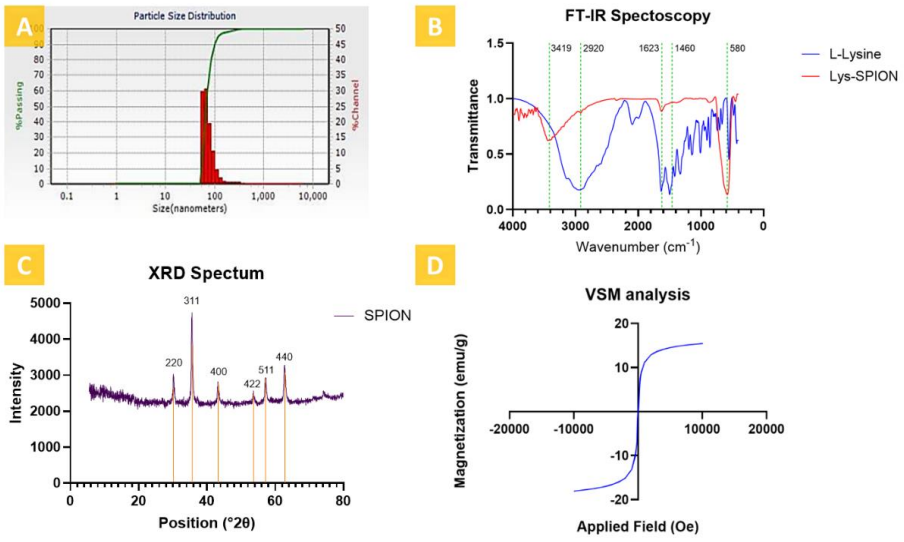

Figure 1. Particle hydrodynamic size distribution (A), FTIR (B), XRD (C), and VSM (D) characteristics of Lys-SPIONS.

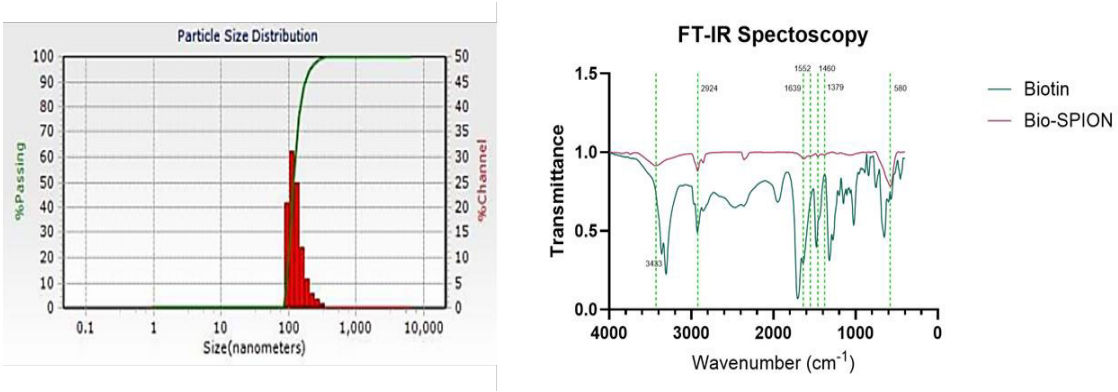

Figure 2. Particle size distribution (left) and FT-IR spectrum (right) of biotinylated SPIONs (Bio-SPION).

cording to this diagram, SPIONs lose their magnetization when the external magnetic field is removed. When an external magnetic field exceeds a specific value, the material magnetization is fixed at a maximum and does not change with a stronger magnetic field.

3.3. Modification of Lys-SPION by Biotin

The melting points of the synthesized biotin-NHS and biotin were determined to be approximately 205 °C and 224 °C, respectively. These values, taking into account non-standard atmospheric conditions and potential impurities, are in line with expected ranges of 212-214 °C and 231-233 °C, at standard atmospheric pressure (17). The 1H-NMR (300 MHz, DMSO-d6) and 13C-NMR (75 MHz, DMSO-d6) spectra of the product (Figure S1) confirmed the formation of biotin-NHS.

Biotinylation increased the hydrodynamic diameter of the NPS to 120 nm (Figure 2) without significantly affecting their zeta potential (Table 1).

A sharp absorption band in the 580 cm-1 region of the FT-IR spectrum is still associated with the strong bond of Fe-O characteristics and indicates the presence of iron oxide nanoparticles (Figure 2). The two absorption bands in the 1552 cm^{-1} and 1639 cm^{-1} regions are related to the stretching vibrations of the C-N bond and the C=O bond of the amide group, respectively. In the spectrum of biotin, a band related to the C-O bond is seen in the 1320 cm^{-1} region, which is eliminated in the spectrum of Bio-SPION (15).

3.4. Superparamagnetic Iron Oxide Nanoclusters (SPINCs)

Complexation of biotin and avidin molecules and formation of nanoclusters induced the sedimentation of nanoparticles, so that the higher the avidin concentration the higher the sedimentation rate of the particles.

Based on the trend of nanocluster formation, the size distribution, and polydispersity index of nanoclusters prepared with different concentrations of avidin (data not shown), a 1:1 mass ratio of nanoparticles to avidin was identified as the optimal ratio. Lower concentrations of avidin (NP to avidin mass ratio ≥ 4) led to incomplete cluster formation, with a substantial number of nanoparticles remaining unclustered. This trend persisted until almost no nanoclusters were formed at NP to avidin

Table 1. Hydrodynamic diameter and zeta potential of iron oxide nanoparticles and iron oxide nanoclusters

Sample	Medium	Hydrodynamic diameter (nm)	Polydispersity Index (PDI)	Zeta Potential (mV)
Lys-SPIONs	Water	67	0.062	- 69.3
Bio-SPIONs	Water	120	0.059	- 62.1
IONCs	water	422	0.080	- 9.1

mass ratios exceeding 20 times.

The hydrodynamic diameter of nanoclusters synthesized with the highest avidin concentration (1:1 Bio-SPION/avidin mass ratio) was measured to be 422 nm (Table 1, Figure 3.A). The positively charged avidin molecules decreased the net charge of the nanoclusters to - 9.1 mV, which does not provide acceptable stability and results in particle sedimentation.

The molar mass ratio of avidin to nanoparticle can be calculated based on the following equation:

$$\frac{Avidin\ mole}{NP\ mole} = \frac{W_{av} \times d_{NP} \times \frac{4}{3}\pi r^3 \times 6.02 \times 10^{-4}}{Mw_{av} \times W_{NP}} \cong 0.2\frac{W_{av}}{W_{NP}} r^3 \qquad \text{(Eq. 1)}$$

Where W is the mass weight of avidin and nanoparticle, dNP is the density of the nanoparticle (equal to 5.17 g/cm^3), r is the radius of the nanoparticle in nanometers, and Mwav is the molar weight of avidin equal to 68.3 kg/mole. In a 1:1 mass ratio or when Wav is equal to WNP then avidin to NP mole ratio is equal to 0.2r^3.

According to Swami et al. study, in the FT-IR spectrum of avidin protein, there is a sharp noticeable absorption band in the region of 1622 cm^{-1} caused by the stretching vibrations of the C=O bond of the amide type I. This peak is visible in the FT-IR spectrum of the fabricated iron oxide nanoclusters at 1629 cm^{-1}. Another notable peak is the absorption band caused by the stretching vibrations of the C=O bond of the amide type II, which is found in the region of 1452 cm^{-1} (Figure 3.B) (18). The electron microscopy image of SPINCs (Figure 3.C) reveals the agglomeration of spherical Bio-SPIONs (Figure S2). The comparison between a single Bio-SPION and a nanocluster seen in Figure 3.C shows an almost 5 times increase in size.

Figure 3.D shows the VSM diagram of iron oxide nanoclusters formed by a 1:1 mass ratio of NPs to avidin compared to Lys-SPIONs at room temperature. The nanoclusters also exhibit a perfect superparamagnetic property. However, their maximum magnetization is higher than the corresponding value in single SPIONs. This means that their magnetic strength in pulling out a trapped biomarker in an applied magnetic field is about twice as

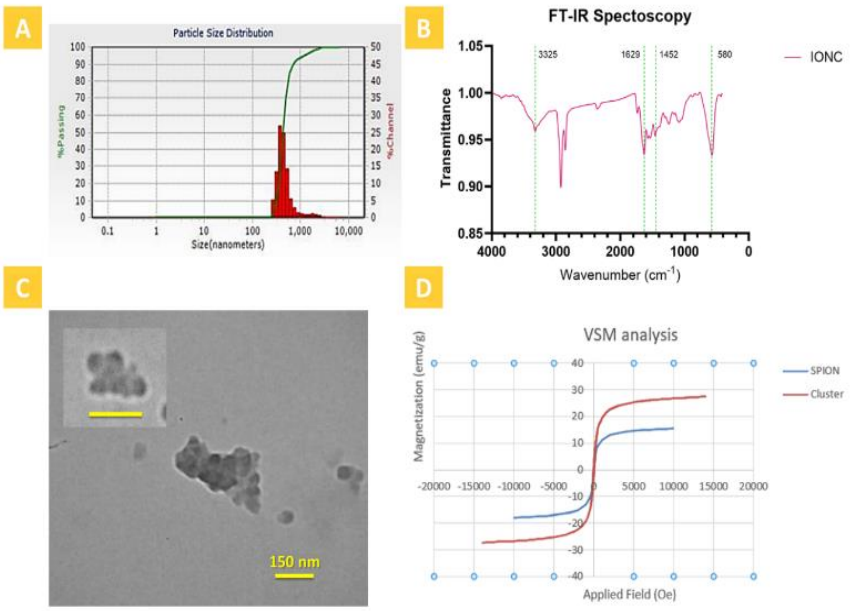

Figure 3. Particle size distribution (A), FT-IR (B), TEM (C), and VSM (D) characteristics of iron oxide nanoclusters formed by 1:1 mass ratio of Bio-Spion to avidin.

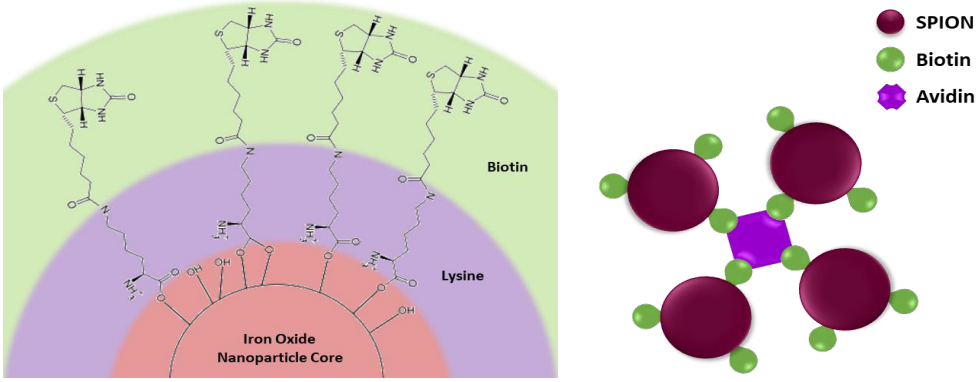

Figure 4. Schematic of possible structure of biotinylated SPION (left) and nanocluster units (right).

high as that of single SPIONs.

4. Discussion

This study aimed to synthesize superparamagnetic iron nanoclusters through biotin-avidin coupling for separating biomarkers from biological environments. The separation and isolation of biological markers using magnetic nanoparticles conjugated with specific ligands offer high sensitivity, specificity, and throughput, making it an economically viable technique. However, challenges arise due to the small size of nanoparticles (like lower strength), which can be partially overcome by optimizing particle size to enhance the quantity and quality of the separation and isolation technique.

In fact, the key feature for isolating biomarkers from biological environments is the superparamagnetic property of nanoparticles, which is dependent on their size. When the particle size of iron oxide exceeds a certain threshold (typically around 15-30 nm), the superparamagnetic property is lost (12, 19). Conversely, reducing the particle size below this threshold diminishes the magnetic strength needed for separating macromolecules like proteins. Hence, the primary challenge lies in enhancing their magnetic strength while preserving the superparamagnetic property.

Clusterization of iron oxide nanoparticles enables controlled size increase while maintaining superparamagnetic properties, making it an efficient tool for optimizing particle size. In this research, a unique method was employed to synthesize iron oxide nanoclusters, enhancing particle size and improving their magnetic strength.

Superparamagnetic iron oxide nanoparticles coated with L-lysine (Lys-SPION) were synthesized using the co-precipitation technique. L-lysine was utilized to create amine (NH_2) functional groups on the nanoparticles as a site for surface modification with biotin. Figure 4 shows the schematic of the possible structure of biotinylated SPION (Bio-SPION) based on the FTIR data analysis. L-lysine can also provide a suitable positive surface charge for nanoparticle stability (14). Subsequently, an amide bond was established between biotin and lysine through the DDC/NHS reaction, allowing the attachment of biotin molecules to the nanoparticle surface. Finally, the addition of avidin macromolecules led to the formation of a biotin-avidin complex, resulting in the aggregation of nanoparticles. By binding up to four biotin molecules from four different nanoparticles to one avidin molecule, iron oxide nanoclusters are formed (Figure 4). The relatively close size of avidin (5 nm) to nanoparticles (<15 nm) facilitates cluster formation by reducing steric hindrance.

DLS analysis of synthetic samples

with varying mass ratios of nanoparticles to avidin revealed a direct correlation between the size of the nanoclusters formed and the concentration of avidin, or more precisely, the mole ratio of avidin to nanoparticles. As the avidin concentration increased, more and larger nanoclusters were observed due to the increased number of connections between avidin and biotin-nanoparticles. Conversely, as the mass ratio of nanoparticles to avidin increased, the likelihood of a reaction between biotin and avidin, leading to nanoparticle clustering, decreased. At mass ratios exceeding 4 times, a significant portion of nanoparticles remain unclustered, and at ratios exceeding 20 times, the majority of nanoparticles exist in a singular state.

The VSM diagram illustrates the magnetic behavior of iron oxide nanoparticles. The point where the diagram intersects the vertical axis is known as remanence magnetization, while the intersection with the horizontal axis is referred to as coercivity (Figure 5) (20). Remanence signifies a material's ability to retain its magnetic properties even after the magnetic field is removed. Non-zero values of magnetic remanence indicate the presence of magnetic properties in a material without the need for an external magnetic field, which is influenced by the microstructural and crystal lattice properties of magnetic materials (21). Coercivity, on the other hand, represents the resistance of a magnetic material to magnetic changes and is essentially the magnetic field required to achieve demagnetization when applied in the opposite direction (22).

The magnetic behavior of particles is influenced by the particle size. Kalubowilage et al. evaluated coercivity against the particle diameter. As evident in Figure 5, up to a specific radius, rsp, the coercivity is zero, indicating the particle completely aligns with the external magnetic field and has no resistance to changes in the magnetic field. This means, in the absence of an external magnetic field, the magnetic property of the particle will also be zero. The value of rsp depends on the type of magnetic material. rsp is considered the boundary between superparamagnetic and ferromagnetic states. As the particle radius exceeds rsp, the coercivity of the particles increases, and the magnetic behavior of the particle changes from superparamagnetic to ferromagnetic, while the particles remain single-domain. This situation continues until a critical radius, called rc, where multiple magnetic domains form within a particle. The maximum coercivity of a particle will be at radius rc, and after that, increasing the number of magnetic domains will reduce the coercivity value (23).

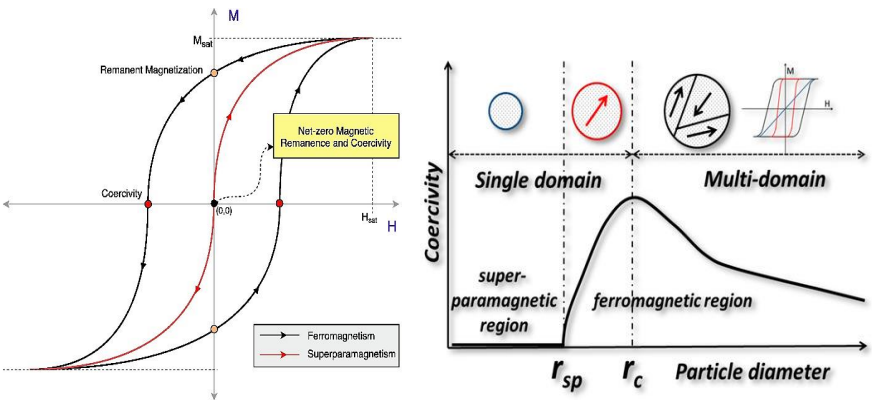

Figure 5. Comparison of magnetization behaviour of ferromagnetic and superparamagnetic materials. Left: reprinted from Sezer et al. paper (20) and demonstration of changes in the magnetic behavior of particles following changes in particle size. Right: reprinted from Kalubowilage et al. paper (23).

Sung Lee et al demonstrated that rsp and rc for iron oxide nanoparticles could be around 30 nm and 100 nm respectively (12).

The VSM results indicated that despite an increase in particle size to approximately 150-200 nm (more than 5 times the superparamagnetic range), the clusters retain their superparamagnetic characteristics (Figure 3). Unlike ferromagnetic materials that gradually lose their magnetic properties in the absence of a magnetic field, displaying remanence magnetism and coercivity with a hysteresis loop in their VSM graph, materials with superparamagnetic behavior rapidly switch between magnetic and non-magnetic states (quickly become magnetic when exposed to magnetic field and lose their magnetic properties at the same rate). This results in a VSM graph with a reversible curve pattern without the formation of a hysteresis loop (Figure 5).

Magnetization is a measure of the magnetic properties of materials, representing the magnetic moment per unit volume in electromagnetic units/cm^3. When an external magnetic field is applied, the material's magnetization increases until it reaches saturation, where it remains constant regardless of further field strength. Saturation magnetization is the maximum magnetization a material can achieve when all its magnetic domains align. This parameter is influenced by atomic properties, magnetic spin alignment, and domain size (24).

Another important quantity to consider is magnetic susceptibility, which represents the change in magnetization per unit increase in magnetic field. It reflects how the magnetic properties or magnetization of a material respond to variations in an external magnetic field. A higher magnetic susceptibility indicates that a material is more likely to reach saturation in lower magnetic fields. The magnetic susceptibility is influenced by the size of magnetic domains, and it decreases as the size of domains grows (24).

The results revealed that following nanoparticles aggregation and cluster formation, the saturation magnetization increased remarkably to approximately twice its initial value, while the susceptibility remained unchanged. This means that the nanoparticles' ability to extract a biomarker from a biological sample is enhanced.

Formation of nanoclusters through biotin-avidin complexes offers several advantages. The high affinity of biotin ligands to avidin proteins enables rapid, cost-effective, and efficient nanocluster formation under simple conditions, eliminating the need for complex laboratory settings. The resulting nanoclusters exhibit desirable thermodynamic stability due to the strong biotin-avidin linkage ($K_a=10^{15}$ M^{-1}).

This method provides precise control over nanocluster size by adjusting the molar ratio of nanoparticles to avidin. Functionalization of nanoparticles and consequent functionalization of nanoclusters with biotin allow for the attachment of various avidinylated or streptavidinylated targeting moieties, creating a versatile platform for separating different biomarkers from biological samples.

An additional advantage of nanocluster formation through biotin-avidin click binding is its reversibility. The structural interaction between biotin and avidin enables the dissociation of constituent nanoparticles, similar to disassembling interlocked puzzle pieces. This can be achieved by introducing extra biotin to the colloid or passing the biotin-avidin complex through a resin column containing avidin/streptavidin macromolecules (25), unlike most nanocluster synthesis methods which are irreversible.

Having hydroxyl groups on the surface, bare iron oxide nanoparticles have a significantly negative zeta potential (26). After coating the particles with L-lysine, the zeta potential of Lys-SPION at pH=7 was measured to be around -69 mV. Biotin has a neutral surface charge, so modifying the nanoparticles with biotin did not affect their surface charge

noticeably. Upon clustering, the surface charge became more positive, reaching -10 mV, attributed to the positive surface charge of avidin protein at pH=7, with an isoelectric value of 10 (27). Zeta potential is crucial for assessing particle stability, as higher positive or negative values indicate increased electrostatic repulsion between particles, leading to slower settling rates and improved physical stability (28). However, the addition of avidin, with its high positive charge, reduced the zeta potential towards zero, decreasing the physical stability of the clusters and causing faster precipitation.

The zeta potential and TGA results (Figure S3) indicate that the number of lysine molecules on the surface of NPs was suboptimal, limiting the available sites for biotin decoration. While the presence of lysine on the surface of SPIONs could slightly alter the zeta potential (as shown in our previous study under review), the amount of lysine amino acid was insufficient to shift the zeta potential of bare SPIONs from negative to positive (due to the amine side chain of lysine). The low biotin content on the nanoparticle surface along with the negative zeta potential, could lead to the formation of nanoclusters primarily through ion interactions rather than biotin-avidin interactions. In other words, ion interactions dominate over the interactions between biotin and avidin molecules. As a result, nanocluster formation was non-uniform to some extent and nanoclusters were irregular and inconsistent in shape. Optimizing the lysine content on the SPIONs surface could be advantageous for attaching the desired quantity of biotin molecules onto the SPIONs, as well as increasing the net charge on the nanoclusters to ensure their colloidal stability.

5. Conclusion

The goal of this project was to explore the potential for enhancing the saturation magnetization of iron oxide nanoparticles without compromising their magnetic susceptibility and superparamagnetic characteristics by creating nanoclusters. We achieved this by generating nanoclusters through a click binding process between biotinylated nanoparticles and avidin. The resulting nanoclusters exhibited favorable magnetic properties and hold potential for further investigation.

Acknowledgements

This work was done as the thesis of Amir Reza Fatemi, financially supported by Shiraz University of Medical Sciences (Grant no. 29373).

Authors contributions

A.R. Fatemi conducted the experimental procedures and wrote the first draft as his thesis project. F. Farvadi reviewed and edited the final draft. She also supervised the project with M.J. Raee. F. Farvadi, A.M. Tamaddon, and D. Firouzabadi contributed to the conceptualization and methodology. S. Sadeghian and S. Amiri were involved in the experimental aspects and data analysis.

Conflict of Interest

The authors declare that they have no conflict of interest.

References

1. Ball JR, Balogh E. Improving Diagnosis in Health Care: Highlights of a Report From the National Academies of Sciences, Engineering, and Medicine. *Ann Intern Med.* 2016 Jan 5;164(1):59-61. doi: 10.7326/M15-2256. Epub 2015 Sep 29. PMID: 26414299.
2. Fairchild A. Palliative radiotherapy for bone metastases from lung cancer: Evidence-based medicine? *World J Clin Oncol*. 2014 Dec 10;5(5):845-57. doi: 10.5306/wjco.v5.i5.845. PMID: 25493222; PMCID: PMC4259946.
3. Safarik I, Safarikova M. Magnetic techniques for the isolation and purification of proteins and peptides. *Biomagn Res Technol*. 2004 Nov 26;2(1):7. doi: 10.1186/1477-044X-2-7. PMID: 15566570; PMCID: PMC544596.
4. Fatima H, Kim K-S. Magnetic

nanoparticles for bioseparation. *Korean J Chem Eng*. 2017;34:589-99.
5. Vangijzegem T, Lecomte V, Ternad I, Van Leuven L, Muller RN, Stanicki D, et al. Superparamagnetic Iron Oxide Nanoparticles (SPION): From Fundamentals to State-of-the-Art Innovative Applications for Cancer Therapy. *Pharmaceutics*. 2023 Jan 10;15(1):236. doi: 10.3390/pharmaceutics15010236. PMID: 36678868; PMCID: PMC9861355.
6. UMN. 2. Classes of Magnetic Materials: University f Minnesota; [cited 2025]. Available from: https://cse.umn.edu/irm/2-classes-magnetic-materials.
7. Olsvik O, Popovic T, Skjerve E, Cudjoe KS, Hornes E, Ugelstad J, Uhlén M. Magnetic separation techniques in diagnostic microbiology. *Clin Microbiol Rev*. 1994 Jan;7(1):43-54. doi: 10.1128/CMR.7.1.43. PMID: 8118790; PMCID: PMC358305.
8. Sun C, Hsieh YP, Ma S, Geng S, Cao Z, Li L, Lu C. Immunomagnetic separation of tumor initiating cells by screening two surface markers. *Sci Rep*. 2017 Jan 11;7:40632. doi: 10.1038/srep40632. PMID: 28074882; PMCID: PMC5225414.
9. Park H, Hwang MP, Lee KH. Immunomagnetic nanoparticle-based assays for detection of biomarkers. *Int J Nanomedicine.* 2013;8:4543-52. doi: 10.2147/IJN.S51893. Epub 2013 Nov 22. PMID: 24285924; PMCID: PMC3841294.
10. Li F, Xu H, Sun P, Hu Z, Aguilar ZP. Size effects of magnetic beads in circulating tumour cells magnetic capture based on streptavidin-biotin complexation. *IET Nanobiotechnol.* 2019 Feb;13(1):6-11. doi: 10.1049/iet-nbt.2018.5104. PMID: 30964030; PMCID: PMC8675959.
11. Antone AJ, Sun Z, Bao Y. Preparation and application of iron oxide nanoclusters. *Magnetochemistry*. 2019;5(3):45.
12. Sung Lee J, Myung Cha J, Young Yoon H, Lee JK, Keun Kim Y. Magnetic multi-granule nanoclusters: A model system that exhibits universal size effect of magnetic coercivity. *Sci Rep.* 2015 Jul 17;5:12135. doi: 10.1038/srep12135. PMID: 26183842; PMCID: PMC4505357.
13. Lyu Y, Martínez Á, D'Incà F, Mancin F, Scrimin P. The Biotin-Avidin Interaction in Biotinylated Gold Nanoparticles and the Modulation of Their Aggregation. *Nanomaterials (Basel)*. 2021 Jun 13;11(6):1559. doi: 10.3390/nano11061559. PMID: 34199307; PMCID: PMC8231960.
14. Raee MJ, Ebrahiminezhad A, Gholami A, Ghoshoon MB, Ghasemi Y. Magnetic immobilization of recombinant E. coli producing extracellular asparaginase: an effective way to intensify downstream process. *Sep Sci Technol.* 2018;53(9):1397-404.
15. Chauhan RP, Singh G, Singh S, Bag N, Patra M, Vadera SR, Mishra AK, Mathur R. Biotinylated magnetic nanoparticles for pretargeting: synthesis and characterization study. *Cancer Nanotechnol.* 2011;2(1-6):111-120. doi: 10.1007/s12645-011-0021-9. Epub 2011 Sep 3. PMID: 26069490; PMCID: PMC4452138.
16. Suhel A, Rahim NA, Rahman MRA, Ahmad KAB. Engine's behaviour on magnetite nanoparticles as additive and hydrogen addition of chicken fat methyl ester fuelled DICI engine: a dual fuel approach. *Int J Hydrog Energy.* 2021;46(27):14824-43.
17. PubChem. National Library of Medicine (NIH); 2025. Available from: https://pubchem.ncbi.nlm.nih.gov/.
18. Swamy MJ, Heimburg T, Marsh D. Fourier-transform infrared spectroscopic studies on avidin secondary structure and complexation with biotin and biotin-lipid assemblies. *Biophys J.* 1996 Aug;71(2):840-7. doi: 10.1016/S0006-3495(96)79285-8. PMID: 8842222; PMCID: PMC1233540.
19. Wu W, Wu Z, Yu T, Jiang C, Kim WS. Recent progress on magnetic iron oxide nanoparticles: synthesis, surface functional strategies and biomedical applications. *Sci Technol Adv Mater.* 2015 Apr 28;16(2):023501. doi: 10.1088/1468-6996/16/2/023501. PMID: 27877761; PMCID: PMC5036481.
20. Sezer N, Arı İ, Bicer Y, Koc M. Superparamagnetic nanoarchitectures: Multimodal functionalities and applications. *J Magn Magn Mater.* 2021;538:168300.
21. Fearon M, Chantrell R, Wohlfarth E. A theoretical study of interaction effects on the remanence curves of particulate dispersions. *J Magn Magn Mater.* 1990;86(2-3):197-206.
22. Givord D, Rossignol M, Barthem VM. The physics of coercivity. *J Magn Magn Mater.* 2003;1;258:1-5.
23. Kalubowilage M, Janik K, Bossmann SH. Magnetic nanomaterials for magnetically-

aided drug delivery and hyperthermia. *Appl Sci*. 2019;9(14):2927
24. Shah SAH. Vibrating sample magnetometery: analysis and construction. Syed Babar Ali School of Science and Engineering, LUMS. 2013.
25. Rybak JN, Scheurer SB, Neri D, Elia G. Purification of biotinylated proteins on streptavidin resin: a protocol for quantitative elution. *Proteomics.* 2004 Aug;4(8):2296-9. doi: 10.1002/pmic.200300780. PMID: 15274123.
26. Durmus Z, Kavas H, Toprak MS, Baykal A, Altınçekiç TG, Aslan A, et al. L-lysine coated iron oxide nanoparticles: synthesis, structural and conductivity characterization. *J Alloys Compd.* 2009;484(1-2):371-6.
27. Jain A, Barve A, Zhao Z, Jin W, Cheng K. Comparison of Avidin, Neutravidin, and Streptavidin as Nanocarriers for Efficient siRNA Delivery. *Mol Pharm.* 2017 May 1;14(5):1517-1527. doi: 10.1021/acs.molpharmaceut.6b00933. Epub 2017 Jan 13. PMID: 28026957; PMCID: PMC6628714.
28. Bhattacharjee S. DLS and zeta potential - What they are and what they are not? *J Control Release.* 2016 Aug 10;235:337-351. doi: 10.1016/j.jconrel.2016.06.017. Epub 2016 Jun 10. PMID: 27297779.